Journal of Sound and Vibration 329 (2010) 4466–4485

Contents lists available at ScienceDirect

Journal of Sound and Vibration

journal homepage: www.elsevier.com/locate/jsvi

Sloshing in partially filled liquid containers—Numerical and experimental study for 2-D problems

P. Pal [a,*], S.K. Bhattacharyya [b]

[a] Department of Civil Engineering, MNNIT Allahabad, Uttar Pradesh 211004, India
[b] Department of Civil Engineering, IIT Kharagpur, Kharagpur 721302, India

ARTICLE INFO

Article history:
Received 19 January 2009
Received in revised form
8 May 2010
Accepted 10 May 2010
Handling Editor: L. Huang
Available online 1 June 2010

ABSTRACT

This paper deals with the numerical and experimental studies of sloshing of liquid in partially filled prismatic containers subjected to external excitation. Meshless local Petrov–Galerkin (MLPG) method is used for computing the nonlinear sloshing response of liquid in a two-dimensional rigid prismatic tank. At every instant of time, velocity potential is computed at each node and the nodal positions are updated. A local symmetric weak form (LSWF) for nonlinear sloshing of liquid is developed, and a truly meshless method, based on LSWF and moving least squares (MLS) approximation, is presented for the solution of Laplace equation with the requisite boundary conditions. An experimental set-up is also designed to study the behavior of liquid sloshing in partially filled prismatic tank. The resulting slosh heights for various excitation frequencies and amplitudes are compared with the data obtained from the numerical studies. The numerical results are close to that obtained experimentally and little variations in the data are due to ineptness of the experimental set-up and the input parameters.

1. Introduction

Liquid in an arbitrary shaped container under external excitations, results in surface and bulk turbulence. The nature of such turbulence is quite complex due to several effects such as sloshing, pressure gradient, etc. Among these, sloshing makes the liquid container more vulnerable to structural damages. Depending on the type of disturbance and container shape, the free liquid surface may experience different types of motion including simple planar, non-planar, rotational, irregular beating, symmetric, asymmetric, quasi-periodic and chaotic. However, the amplitude of slosh depends on the amplitude and frequency of the tank motion, liquid-fill depth, liquid properties and tank geometry. Hence liquid sloshing is a practical problem with regard to the safety of transportation systems, such as oil tankers on highways, liquid tank cars on railroads, oceangoing vessels with liquid cargo, propellant tank used in satellites and other spacecraft vehicles, and several others.

Simulation of sloshing of liquid has received attention of several researchers. Different numerical schemes such as finite difference method (FDM), finite volume method (FVM), boundary element method (BEM), finite element method (FEM), etc. are employed to solve the coupled fluid–structure systems. These methods have provided many useful and satisfactory results. However, the success of these methods depends primarily on the refinement of the meshes. It is well known that the construction of such precise meshes is usually difficult and time-consuming task. In addition, elements can frequently

* Corresponding author. Tel.: +919451071844.
E-mail addresses: prpal2k@gmail.com (P. Pal), bsri@civil.iitkgp.ernet.in (S.K. Bhattacharyya).

0022-460X/$ - see front matter © 2010 Elsevier Ltd. All rights reserved.
doi:10.1016/j.jsv.2010.05.006

Nomenclature

a_h	applied amplitude (m)
B	breadth of the tank (m)
g	acceleration due to gravity (m/s^2)
h_l	depth of liquid into the tank (m)
H	height of the tank (m)
L	width of the tank (m)

Greek letters

ζ	sloshing amplitude (m)
ρ_f	mass density of liquid (kg/m^3)
ω	sloshing frequency (numerical, rad/s)
ω_h	applied frequency (rad/s)
ω_{ns}	sloshing frequency (experimental, rad/s)

become over-distorted during the simulation of liquid sloshing. So the employment of conforming meshes for the solution of sloshing phenomenon is not quite suitable for design purposes, as the spatial grid of the geometric model restrict changes of the parameters, it is difficult or even impossible to change the shape of the model without remeshing. To overcome these problems, the focus of research is directed on the development of alternative techniques, which do not have an explicit boundary between the pre-process and the main process. In particular, the meshless methods, and a number of techniques have been recently proposed by different researchers. Various meshless methods belonging to this family are as follows: smooth particle hydrodynamics (SPH) [1], diffuse element method (DEM) [2], element-free Galerkin (EFG) method [3], reproducing kernel particle method (RKPM) [4], the partition of unity (PU) method [5] and meshless local Petrov–Galerkin (MLPG) method [6]. In one of such approaches, the meshless local Petrov–Galerkin (MLPG) method based on MLS approximations, proposed by Atluri and his coworkers has been successfully developed. Atluri and Shen [7,8] discussed the generality of MLPG approach, based on either symmetric or unsymmetric weak forms, and using different types of meshless interpolations of trial functions, as well as different types of meshless interpolation of test functions. The authors presented the weak forms as the basis of a variety of numerical methods, such as FVM, FEM and BEM.

In the last few decades researchers have investigated sloshing of liquid numerically as well as experimentally. The special NASA monograph edited by Abramson [9] addressed the sloshing problems encountered in aerospace vehicles. The monograph contained the analytical and experimental studies of linear, nonlinear sloshing, damping of liquid motions, vertical excitations of tanks, interaction of liquid propellants and elastic structures, vehicle stability and control, liquid propellant behavior at low and zero gravity, longitudinal oscillation of flight vehicles, etc. Wu et al. [10] analyzed the sloshing waves in a three dimensional tank using finite element method based on fully nonlinear wave potential theory. The authors provided extensive results for sloshing waves in a 3D tank subjected to translation motions. Pal et al. [11] conducted experimental studies on the sloshing response of liquid-filled containers. A three-dimensional finite element analysis was carried out for the numerical simulation of the problem [12] considering nonlinear free surface wave. The effects of sloshing were computed in the time domain using Newmark's time integration scheme. A simple experimental set-up was designed and fabricated to conduct experiments for measuring some of the basic parameters of sloshing. A sensor device was developed to record the free-surface wave heights. Each wave height sensor was a capacitance probe that detected the change in level of liquid (water) precisely with no time lag. Celebi and Akyildiz [13] presented a nonlinear liquid sloshing inside a partially filled rectangular tank using finite difference approximations. At each time step, the technique was used to track the locations of the free surface. The fluid was assumed as homogeneous, isotropic, viscous, Newtonian and compressible. Biswal et al. [14] presented the natural frequencies of liquid in a liquid-filled cylindrical rigid tank with or without baffles. The authors used an annular plate as a baffle, which was fitted to the inner periphery of a cylindrical tank. Both rigid and flexible baffles were considered into the computation. Finite element technique was used to solve both the liquid and the structural domain. Frandsen [15] presented a fully nonlinear finite difference model based on inviscid flow equations. The author considered several numerical experiments in a 2-D tank which was excited both horizontally and vertically. Results of liquid sloshing induced by harmonic base excitations were presented for small to steep non-breaking waves. A methodology for nonlinear water wave problems using MLPG approach was presented by Ma [16]. The Navier–Stokes equations for incompressible and inviscid fluid and a time marching procedure were used in the formulation. Heaviside step function was considered in the formulation as a test function. Ma [17] developed the MLPG method into a new form, i.e. the MLPG_R method for modeling the nonlinear water wave problems. The solution for Rankine sources was considered in the formulation as the test function. Numerical results showed that the MLPG_R method could be twice as fast as the MLPG method for modeling the nonlinear water wave problems. Biswal et al. [18] presented the nonlinear sloshing response of liquid in a two-dimensional rigid rectangular container with rigid baffles. A finite element technique was used to solve the nonlinear potential problems. The authors solved the nonlinear sloshing problems in a circular cylindrical container with annular baffle. Ma [19] presented a new meshless interpolation scheme for meshless local Petrov–Galerkin method based on Rankine source solution (MLPG_R). In this scheme, the author formulated a simplified finite difference interpolation to discretize the governing equation. The new scheme was developed with less computational efforts, and to enhance the overall efficiency of the MLPG_R method. Ma and Zhou [20] extended the previous work to simulate breaking waves using meshless local Petrov–Galerkin method based on Rankine source solution. Authors suggested here a new approach for identifying the free surface particles.

The focus of the present study is on the development of a MLPG formulation based on LSWF with MLS approximation for solving the nonlinear free surface oscillation in two-dimension. A finite difference based iterative time stepping technique is employed to advance the solution in the time domain. From the solution of the velocity potential and velocity vector at a given time step at a given iteration, the resulting values of the hydrodynamic pressure in the liquid domain and the updated position of the free surface at the start of the next iteration are obtained. Computer codes using FORTRAN are developed for the purpose. The computed code is then verified by comparing the calculated results with the published data, and good agreement is found. An experimental set-up is designed to study the behavior of liquid sloshing in partially filled prismatic tank. The resulting slosh heights for various excitation frequencies and amplitudes are compared with the existing results and the data obtained from the numerical studies.

2. Theoretical formulation

2.1. Governing equations for the liquid domain

Fig. 1 shows the problem geometry of a typical 2-D prismatic shaped partially liquid-filled rigid container having a width (L) and height (H). The depth of liquid is h_l. The contained liquid is assumed to be incompressible and inviscid resulting in an irrotational flow field. The bottom of the tank is assumed as rigidly fixed to the base. The analysis of the nonlinear free surface flow problem is based on the potential flow theory. The entire flow field is described by a scalar function called velocity potential $\phi(x,z,t)$, which satisfies the Laplace equation

$$\nabla^2\phi(x,z,t)=0 \tag{1}$$

Eq. (1) is solved using the MLPG technique with the appropriate time-dependent boundary conditions [18] as specified below:

(a) *At the liquid–structure interface*:

$$\frac{\partial\phi}{\partial n}=v_n \quad \text{on } \Gamma_i \tag{2}$$

where v_n is the normal velocity of the structure, and n is the normal of the surface pointing out of the liquid domain.

(b) *At the liquid free surface* (Γ_f):

The kinematic and dynamic boundary conditions on the liquid free surface are

$$\frac{\partial\phi}{\partial z}=\frac{\partial\eta}{\partial t}+\frac{\partial\phi}{\partial x}\frac{\partial\eta}{\partial x} \tag{4}$$

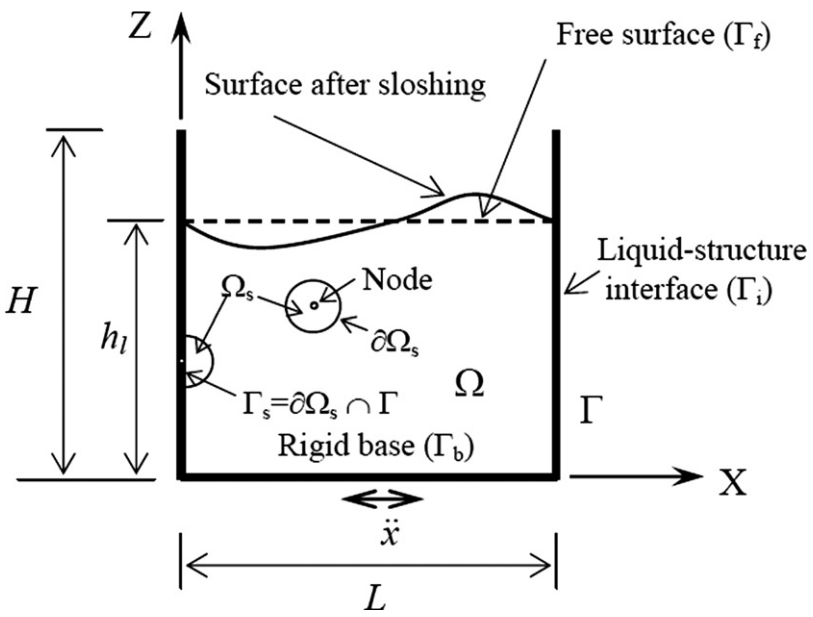

Fig. 1. Model used for analysis.

and

$$\frac{\partial\phi}{\partial t}+\frac{1}{2}(\vec{\nabla}\phi\cdot\vec{\nabla}\phi)+g\eta=0 \tag{5}$$

where g is the gravitational acceleration and η is the free surface displacement. The atmospheric pressure on the free surface has been taken as zero in Eq. (5).
Noting that

$$\frac{\mathrm{d}x}{\mathrm{d}t}=\frac{\partial\phi}{\partial x}\quad\text{and}\quad\frac{\mathrm{d}z}{\mathrm{d}t}=\frac{\partial\phi}{\partial z} \tag{6}$$

Eq. (5) may be expressed in the Lagrangian form as

$$\frac{\mathrm{d}\phi}{\mathrm{d}t}=-g\eta+\frac{1}{2}(\vec{\nabla}\phi\cdot\vec{\nabla}\phi) \tag{7}$$

(c) *At the bottom of the tank*:

$$\frac{\partial\phi}{\partial n}=0\quad\text{on }\Gamma_b \tag{3}$$

The hydrodynamic pressure of the excited liquid may be obtained from Bernoulli's equation as

$$\frac{p(x,z,t)}{\rho_f}=-\left[\frac{\partial\phi}{\partial t}+\frac{1}{2}(\vec{\nabla}\phi\cdot\vec{\nabla}\phi)+g\eta\right] \tag{8}$$

where ρ_f is the mass density of liquid. Eqs. (1)–(5) define the initial and the boundary value problem, which are Laplace equation with nonlinear boundary conditions imposed on the free surface. Here the nonlinearity [12] manifests itself in two ways:

i. The elevation of the moving free surface is not known a priori at any given time instant.
ii. The boundary conditions on the free surface (i.e. Eqs. (4) and (5)) contain second-order differential terms.

2.2. The meshless local Petrov–Galerkin (MLPG) formulation

2.2.1. The MLS approximation scheme

A sub-domain Ω_x, the neighborhood of a point x, denoted as the domain of definition of MLS approximation for the trial function at x, is located in the problem domain Ω. In Fig. 2, the local domains, the supports of nodes, the domain of

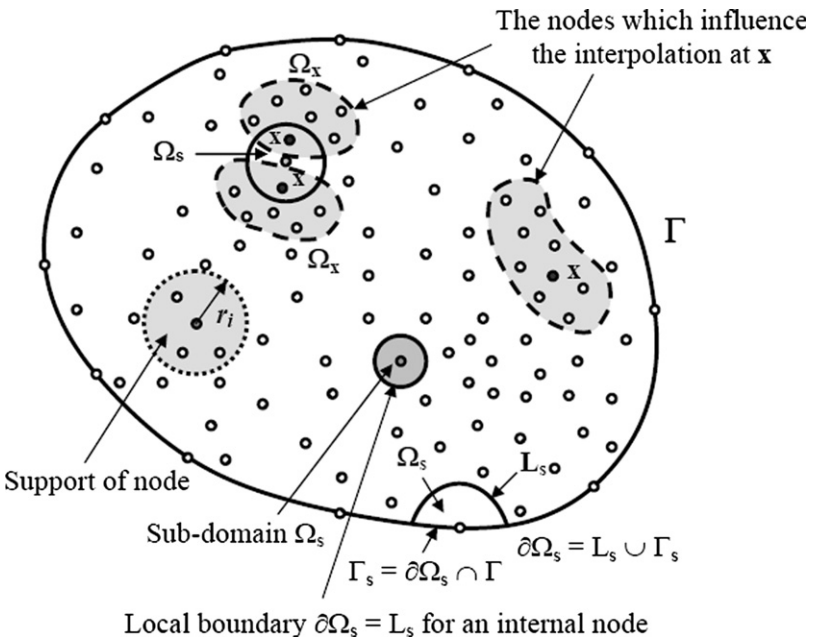

Fig. 2. Schematics of the MLPG.

definition of the MLS approximation for the trial function at a point and the domain of influence of a source point are defined. To approximate the distribution of function u in Ω_x over a number of randomly located nodes $\{x_i\}$, $i=1,2,\ldots,n$, the moving least squares approximant $u^h(x)$ of u, for all $x\in\Omega_x$, may be defined as

$$u^h(x)=\sum_{j=1}^{m}P_j(x)a_j(x)\equiv P^T(x)a(x)\quad \forall x\in\Omega_x \tag{9}$$

where $P_j(x)$, $j=1, 2,\ldots,m$ are complete monomial basis of order m. The co-efficient vector $a(x)$ is determined by minimizing a weighted discrete L_2 norm of error function $J(x)$, defined as

$$J(x)=\sum_{i=1}^{n}v_i(x)\left[P^T(x_i)a(x)-u_i\right]^2 \tag{10}$$

where $v_i(x)$ is the weight function associated with node i, with $v_i(x)>0$ for all x in the support of $v_i(x)$. The stationarity of $J(x)$ in Eq. (10) with respect to $a(x)$ leads to the following linear relation [6] between $a(x)$ and u_i.

$$[A]\{a\}=[B]\{u\} \tag{11}$$

where $[A]$ and $[B]$ are the matrices obtained from both trial and test functions. Solving the $a(x)$ from Eq. (11) and substituting the same in Eq. (9), a relation in the form of an interpolation function similar to that used in FEM, is obtained as

$$u^h(x)=\sum_{i}^{n}\sum_{j}^{m}P_j(x)(A^{-1}(x)B(x))_{ji}u_i\equiv\sum_{i}^{n}N_i(x)u_i \tag{12}$$

where the shape function $N_i(x)$ is defined as

$$N_i(x)=\sum_{j=1}^{m}P_j(x)(A^{-1}(x)B(x))_{ji}=P^TA^{-1}B \tag{13}$$

The smoothness of the shape functions is determined by that of the basis functions and of the weight functions. The Gaussian type weight function with compact support is considered in the present study. The Gaussian weight function corresponding to node i may be written as

$$v_i(x)=\begin{cases}\dfrac{\exp\left[-(d_i/c_i)^{2k}\right]-\exp\left[-(r_i/c_i)^{2k}\right]}{1-\exp\left[-(r_i/c_i)^{2k}\right]} & 0\le d_i\le r_i\\ 0 & d_i\ge r_i\end{cases} \tag{14}$$

where $d_i||x-x_i||$ is the distance from node x_i to point x. c_i is a constant controlling the shape of the weight function v_i. r_i is the size of the support for the weight function v_i and it determines the support of node x_i. In the present work, $k=1$ is chosen for C^0 continuity over the entire domain Ω. The size of support of the weight function v_i associated with node i should be chosen such that r_i should be large enough to have sufficient number of nodes covered in the domain of definition of every sample point ($n\ge m$) to ensure the regularity of $[A]$. The value of c_i is chosen in such a way that the size (radius) of each local sub-domain should be big enough so that the union of all local sub-domains covers as much as possible of the global domain.

2.2.2. Local symmetric weak form (LSWF)

The MLPG technique is used to solve the Laplace equation (Eq. (1)), where ϕ is the velocity potential, which is considered as the trial function in the formulation. The domain Ω is enclosed by $\Gamma=\Gamma_\phi\cup\Gamma_q$ with boundary conditions. The essential and natural boundary conditions are given as

$$\phi=\overline{\phi}\quad\text{on }\Gamma_\phi,\quad \frac{\partial\phi}{\partial n}\equiv q=\overline{q}\quad\text{on }\Gamma_q \tag{15}$$

where $\overline{\phi}$ and $\overline{q}$ are the prescribed potential and normal flux, respectively, on the essential boundary Γ_ϕ and on the flux boundary Γ_q and n is the outward normal direction to the boundary Γ.

A generalized local weak form of the differential Eq. (1) and the boundary conditions of Eq. (15), over a local sub-domain Ω_s [6], may be written as

$$\int_{\Omega_s}\nabla^2\phi v\,d\Omega-\alpha\int_{\Gamma_{s\phi}}(\phi-\overline{\phi})v\,d\Gamma=0 \tag{16}$$

where ϕ is the trial (basis) function, v is the test (weight) function and $\Gamma_{s\phi}$ is a part of the boundary $\partial\Omega_s$ of Ω_s (Γ_s in Fig. 2), over which the essential boundary conditions are specified. In general, $\partial\Omega_s=\Gamma_s\cup\Gamma_s$, with Γ_s being a part of the local boundary located on the global boundary and L_s being the other part of the local boundary over which no boundary condition is specified, i.e. $\Gamma_s=\partial\Omega_s\cup\Gamma$ and $L_s=\partial\Omega_s-\Gamma_s$. If the sub-domain Ω_s is located entirely within the global domain Ω, and there is no intersection between the local boundary $\partial\Omega_s$ and the global boundary Γ, the boundary integral over $\Gamma_{s\phi}$

vanishes. In Eq. (16), a penalty parameter $\alpha \gg 1$ is used to impose the essential boundary conditions. Using $(\nabla^2\phi)v = \phi_{,ii}v = (\phi_{,i}v)_{,i} - \phi_{,i}v_{,i}$, the divergence theorem, the following expression is obtained:

$$\int_{\partial\Omega_s} \phi_{,i} n_i v \, d\Gamma - \int_{\Omega_s} \phi_{,i} v_{,i} \, d\Omega - \alpha \int_{\Gamma_{s\phi}} (\phi - \overline{\phi}) v \, d\Gamma = 0 \tag{17}$$

in which $\partial\Omega_s$ is the boundary of the sub-domain Ω_s and n is the outward unit normal to the boundary $\partial\Omega_s$. Imposing the natural boundary condition, $q = \overline{q}$ and noting that $\phi_{,i} n_i = \partial\phi/\partial n \equiv q$ in Eq. (17), the following expression is obtained:

$$\int_{L_s} q v \, d\Gamma - \int_{\Gamma_{s\phi}} q v \, d\Gamma - \int_{\Gamma_{sq}} \overline{q} v \, d\Gamma - \int_{\Omega_s} \phi_{,i} v_{,i} \, d\Omega - \alpha \int_{\Gamma_{s\phi}} (\phi - \overline{\phi}) v \, d\Gamma = 0 \tag{18}$$

in which Γ_{sq} is a part of $\partial\Omega_s$, over which the natural boundary condition is specified. For a sub-domain located entirely within the global domain, there is no intersection between $\partial\Omega_s$ and Γ, $L_s = \partial\Omega_s$ and the integrals over $\Gamma_{s\phi}$ and Γ_{sq} vanish. Using the test function and rearranging the Eq. (18), the following local symmetric weak form (LSWF) is obtained:

$$\int_{\Omega_s} \phi_{,i} v_{,i} \, d\Omega + \alpha \int_{\Gamma_{s\phi}} \phi v \, d\Gamma - \int_{\Gamma_{s\phi}} q v \, d\Gamma = \int_{\Gamma_{sq}} \overline{q} v \, d\Gamma + \alpha \int_{\Gamma_{s\phi}} \overline{\phi} v \, d\Gamma \tag{19}$$

In concise form of Eq. (19) leads to the following discretized system of linear equations:

$$[K]\{\phi\} = \{F\} \tag{20}$$

where $[K]$ and $\{F\}$ are the liquid stiffness matrix and the liquid load vector, respectively, and are defined as

$$K_{ij} = \int_{\Omega_s} N_{j,k} v_{,k} \, d\Omega + \alpha \int_{\Gamma_{s\phi}} N_j v \, d\Gamma - \int_{\Gamma_{s\phi}} N_{j,n} v \, d\Gamma \tag{21}$$

$$F_i = \int_{\Gamma_{sq}} \overline{q} v \, d\Gamma + \alpha \int_{\Gamma_{s\phi}} \overline{\phi} v \, d\Gamma \tag{22}$$

where v is the weight function and N_j is the shape function obtained from MLS approximation, and $(\,)_{,n} = \partial(\,)/\partial n$. The velocity potential in the domain is obtained from Eq. (20). A finite difference based iterative time stepping technique is used to advance the solution in the time domain. The updated position of the free surface may be obtained by using Eq. (6) and the updated velocity potential on the free surface is obtained from Eq. (7). The liquid domain is updated based on the positions of newly formed messless nodes.

3. Numerical examples and results

The characterization of sloshing behavior, evaluation of liquid frequencies, mode shapes, and forced response characteristics in two-dimensional prismatic containers are addressed in this section. The governing equations along with the detailed theoretical formulations based on MLPG technique and the solution procedures are presented in Section 2. A number of examples are presented herein to validate the developed computer code and to establish the applicability of the algorithm to a wide variety of sloshing problems. Simple harmonic oscillations are used as external excitation in the example problems. It may be noted that if the disturbance of the free surface is small in magnitude in comparison to the depth and the wave length of liquid, the free surface conditions may be linearized. The nonlinear effects arising as a consequence of a relatively large amplitude motion near resonance are also discussed in this section.

In the present investigation, the Petrov–Galerkin technique is used in each local sub-domain. In the conventional Galerkin method, the trial and test functions are chosen from the same space, however, in the Petrov–Galerkin method, the trial and test function are used from different spaces. In the present study, the size (radius) of test function is chosen as equal to the minimum nodal spacing between two consecutive nodes into the global domain whereas the size (radius) of trial function is considered as equal to that of the size of test function multiplied by the scaling parameter.

A regular distribution of nodes is used to discretize the liquid domain in two-dimension with velocity potential as the unknown nodal variable. For 2-D problem, if the distribution of nodes is same in both the directions, the nodal spacing will be identical and the computed size of test and trial functions becomes well defined. If the distributions are otherwise, the size of test function will be the least distance between any two consecutive nodes. Also a suitable scaling parameter is required to be established to arrive at an appropriate size of trial function. For such case, the computation of trial function size becomes difficult as a well defined shape function needs greater number of nodes than the polynomial degree. Therefore the regular distributions of nodes (same in both directions) are employed in order to achieve the computational accuracy. Hence, the rate of convergence of the solution depends on the nodal distributions, and on the size of sub-domain, which are computed using the scaling parameter.

The total number of nodes in the global domain is chosen in such a way that the union of all local sub-domains cover the global domain as much as possible with minimum intersection of sub-domains. If more number of nodes is added in the global domain, the more integration points are required to achieve the computational accuracy corresponding to a smaller nodal distance. This kind of difficulty may cause the complexity of the shape functions in the MLPG method. So it will be facilitative in the computation of the MLPG method, if the nodal spacing in both the directions (2-D case) is same.

In the computation, the size of support for the weight function is taken to be $2h$ to $3h$ with h being the distance between two consecutive nodes and the constant controlling parameter c_i for Gauss weight function is assumed as $r_i/4$. The radius of size of supports $r_i=s_ih$ where s_i is the scaling parameter. Nine (9) Gauss points are used on each section of boundary and 8×8 Gauss points are used in the local domain for numerical quadrature. The material properties of the liquid domain considered are

Mass density of liquid,	$\rho_f=1000$ kg/m^3
Gravitational acceleration,	$g=9.81$ m/s^2

A convergence study is carried out to find out the appropriate scaling parameter and the number of nodes required to achieve minimum error in the evaluated sloshing frequency. A parametric study is also carried out to observe the effect of liquid depth on the computed liquid sloshing frequency.

Example 1. Inappropriate choice of scaling parameter in the weight function leads to the unsatisfactory results. This example is studied to find out the appropriate scaling parameter for the problem considered herein. The width (L) of the container is 1.0 m and the liquid depth (h_l) is 1.0 m. These dimensions are considered similar to the ones, available in literature [9], for comparison. Fig. 3 shows the error level in the computation of first natural sloshing frequency of liquid for different scaling parameters. The error norm for the frequency is evaluated as follows:

$$||e|| = \left|\frac{f_1-f_2}{f_1}\right| \tag{23}$$

where f_1 is the analytical frequency and f_2 is the computed frequency. Based on this study, scaling parameter values of 2.125 for linear Gauss (LG) weight function and 2.2 for linear Spline (LS) weight function are chosen for the present solution. It is observed that MLPG codes give better results with the use of Gaussian weight function instead of the Spline weight function.

Example 2. This example is considered to observe the total number of nodes required to achieve minimum error in the evaluated sloshing frequency. The width of container and the depth of liquid considered are same as presented in Example 1. The percentage error norm for the frequency is evaluated using Eq. (23). The distribution of nodes is made in such a manner that the nodal spacing in both the directions is same. The scaling parameter is considered as 2.125. Fig. 4 shows the variation of percentage error norm with the variation of number of nodes. It is observed that at the selection of 81 nodes, the computed frequency is converged with the analytical ones. The required total number of nodes also may be selected based on the error norm of amplitude of waves.

In order to achieve the minimum computational error, the scaling parameter is selected based on the minimum distance between two consecutive nodes distributed in the problem domain. So the above two examples are correlated. Based on the above observations the following examples are studied and compared with the reported results.

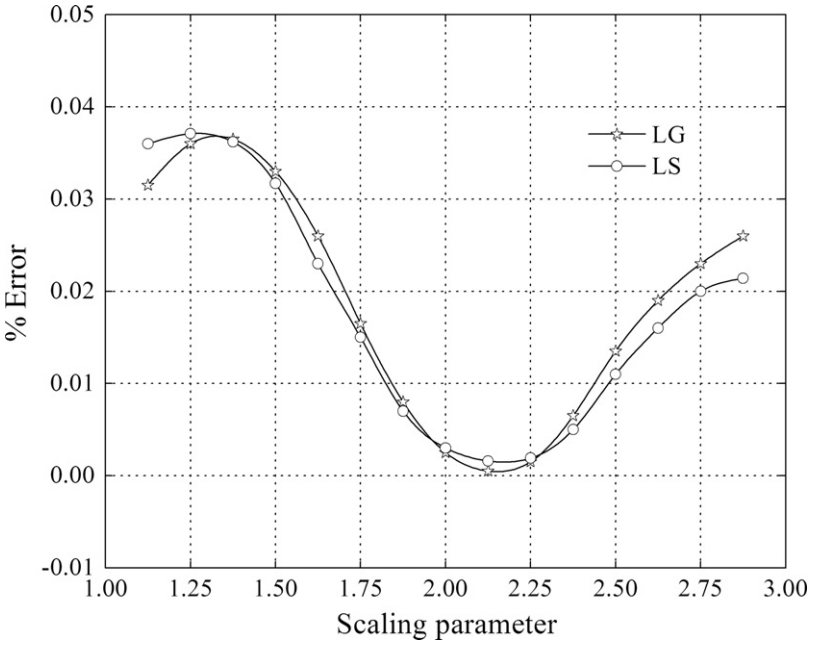

Fig. 3. Relative error with scaling parameter for potential flow problem.

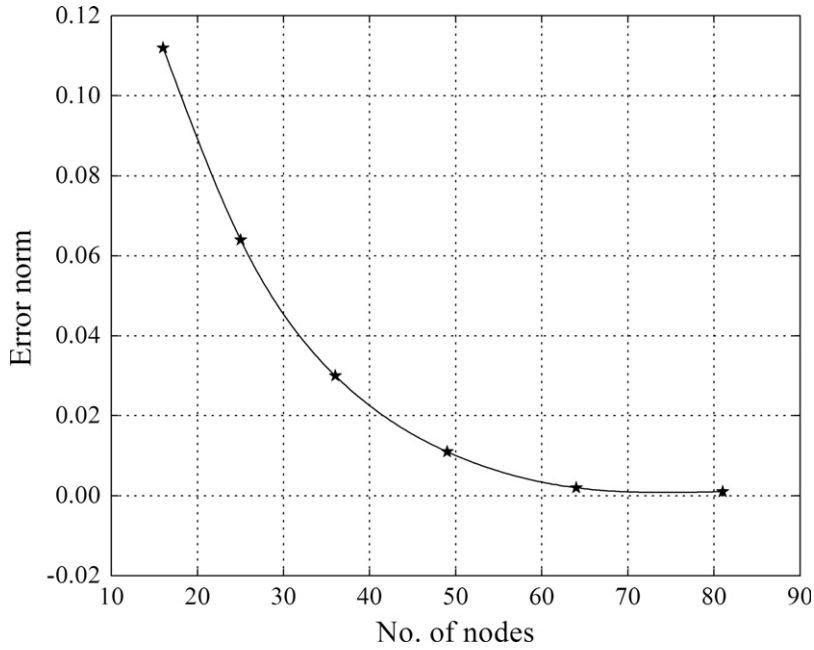

Fig. 4. Percent error norm variation corresponding to the number of nodes.

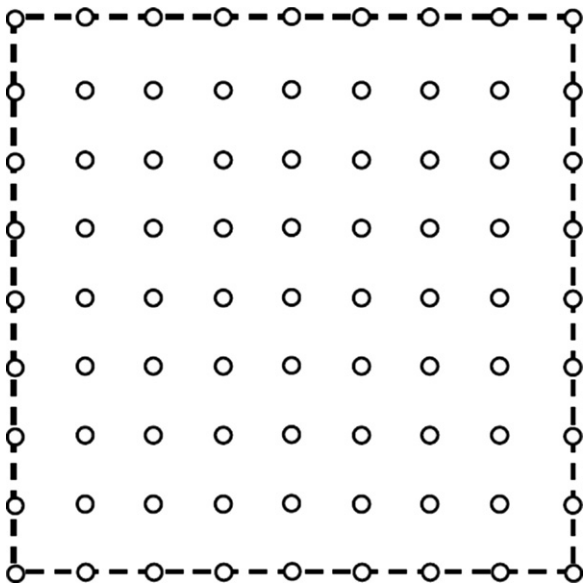

Fig. 5. Liquid domain with 9×9 regular nodes.

Example 3. The evaluation of slosh frequencies of liquid is addressed in this example. The width of container is 1.0 m and depth of liquid is 1.0 m. The scaling parameter is chosen as 2.125. Regular distribution of 81 (9×9) nodes is used to study the convergence of the present MLPG method, as shown in Fig. 5. The computed liquid slosh frequencies and different modes are presented in Table 1. The natural mode shapes for the liquid at the mean surface are shown in Fig. 6. It is observed that the present results are in good agreement with the reported results by Abramson [9] and Pal et al. [11].

Example 4. In this example, it is intended to study the effect of liquid depth on the computed liquid slosh frequency. The width (L) of the container is fixed as 1.0 m. Fig. 7 illustrates the variation of slosh frequencies of prismatic container for

different values of liquid depth (h_l) to the base width (L) ratio. It is observed that the frequencies of the liquid decrease with decreasing liquid depth. However, the frequencies of each mode are same when h_l/L approaches unity.

Based on the comparative studies, it is ascertained that the present MLPG codes give the satisfactory results. The developed codes are then used to compute the liquid displacements for a prescribed excitation.

Example 5. To validate the present computational algorithm, the transient effects of both linear and nonlinear free surface condition of a liquid-filled prismatic container in two-dimension are observed. The similar problem was solved by Washizu et al. [21] using the FEM approach and is available in the literature. The width (L) of the container is 1.0 m and the liquid

Table 1
Slosh frequencies, f_n (Hz) of liquid in a prismatic container.

Mode	Abramson [9] (analytical)	Pal et al. [12] (FEM)	Present study (MLPG)
1	0.88	0.88	0.883
2	1.24	1.26	1.253
3	1.53	1.54	1.545
4	1.76	1.80	1.786

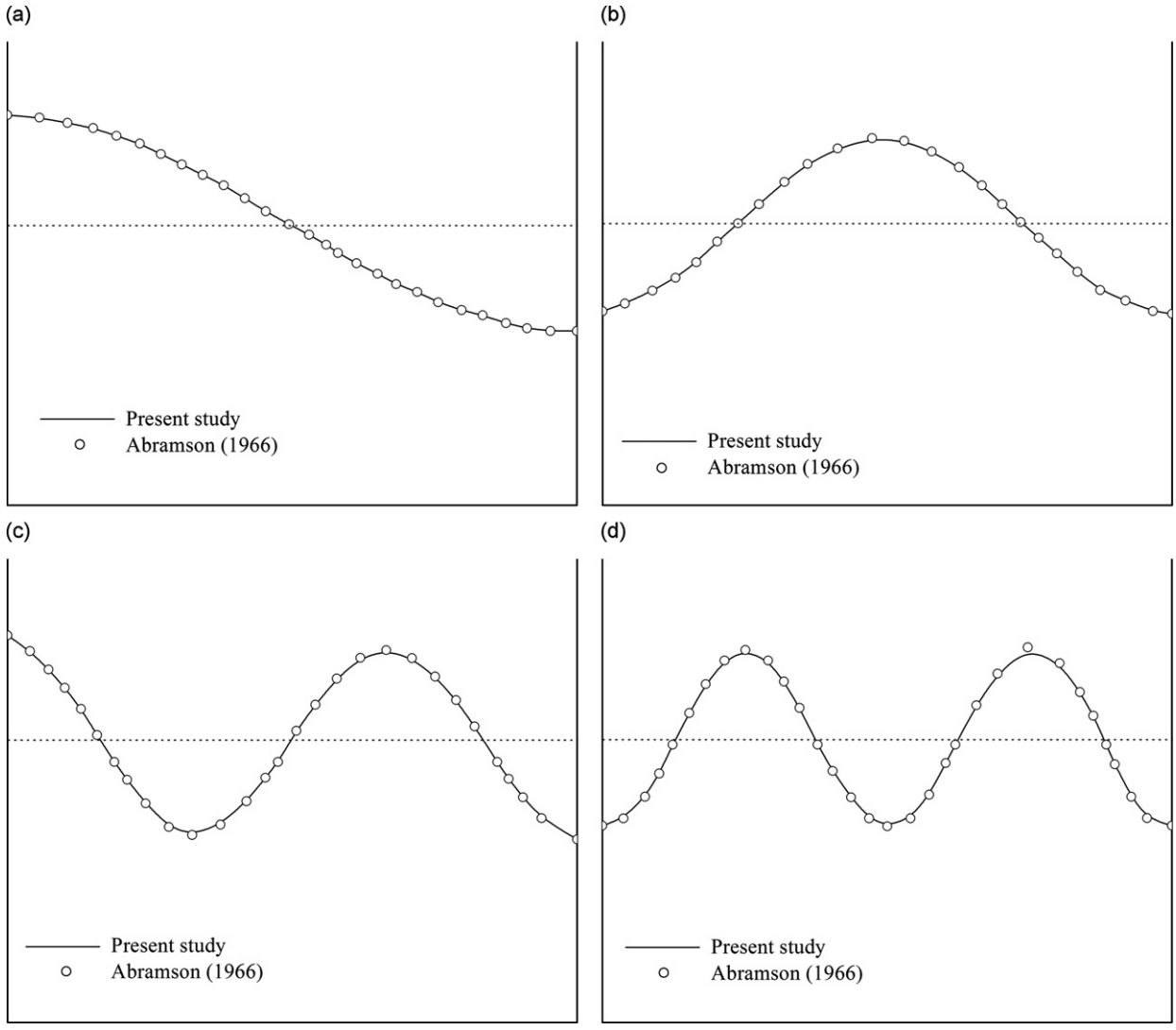

Fig. 6. Natural mode shapes of liquid free surface: (a) mode 1, (b) mode 2, (c) mode 3 and (d) mode 4.

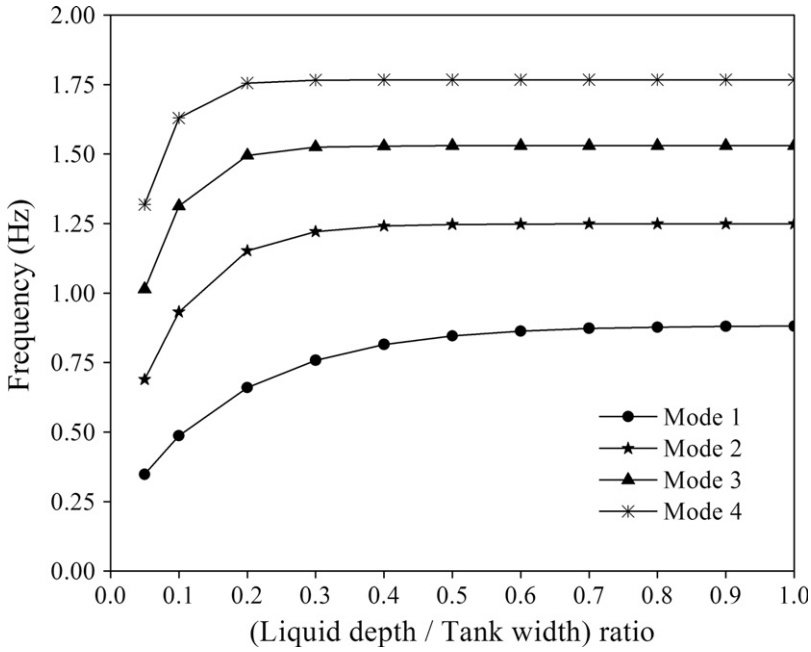

Fig. 7. Variation of sloshing frequencies with different liquid depth to container width ratio.

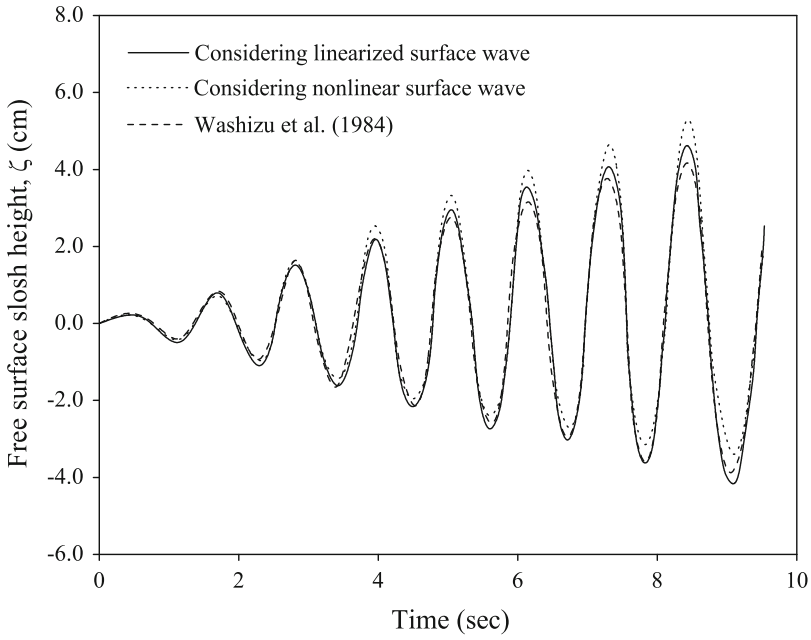

Fig. 8. Slosh displacements in a prismatic container under sinusoidal base excitation.

depth (h_l) is 1.0 m. It is subjected to a sinusoidal forced horizontal acceleration of the type given as

$$\ddot{x}(t) = -X_0\omega^2 \sin\omega t \quad \text{for } t \geq 0 \tag{24}$$

where X_0 and ω are the amplitude and the frequency of the forced horizontal acceleration, respectively. The parameters X_0 and ω are 0.002 m and 5.55 rad/s, respectively. Typical time response of the free surface slosh amplitude near the outer wall of the container is shown in Fig. 8. The response shown in figure appears to match closely with that of Washizu et al. who had earlier solved this problem using the nonlinear free surface boundary condition. The results show some difference when considering nonlinear effect of the surface wave. It may be caused due to the effect of scaling parameter value in the

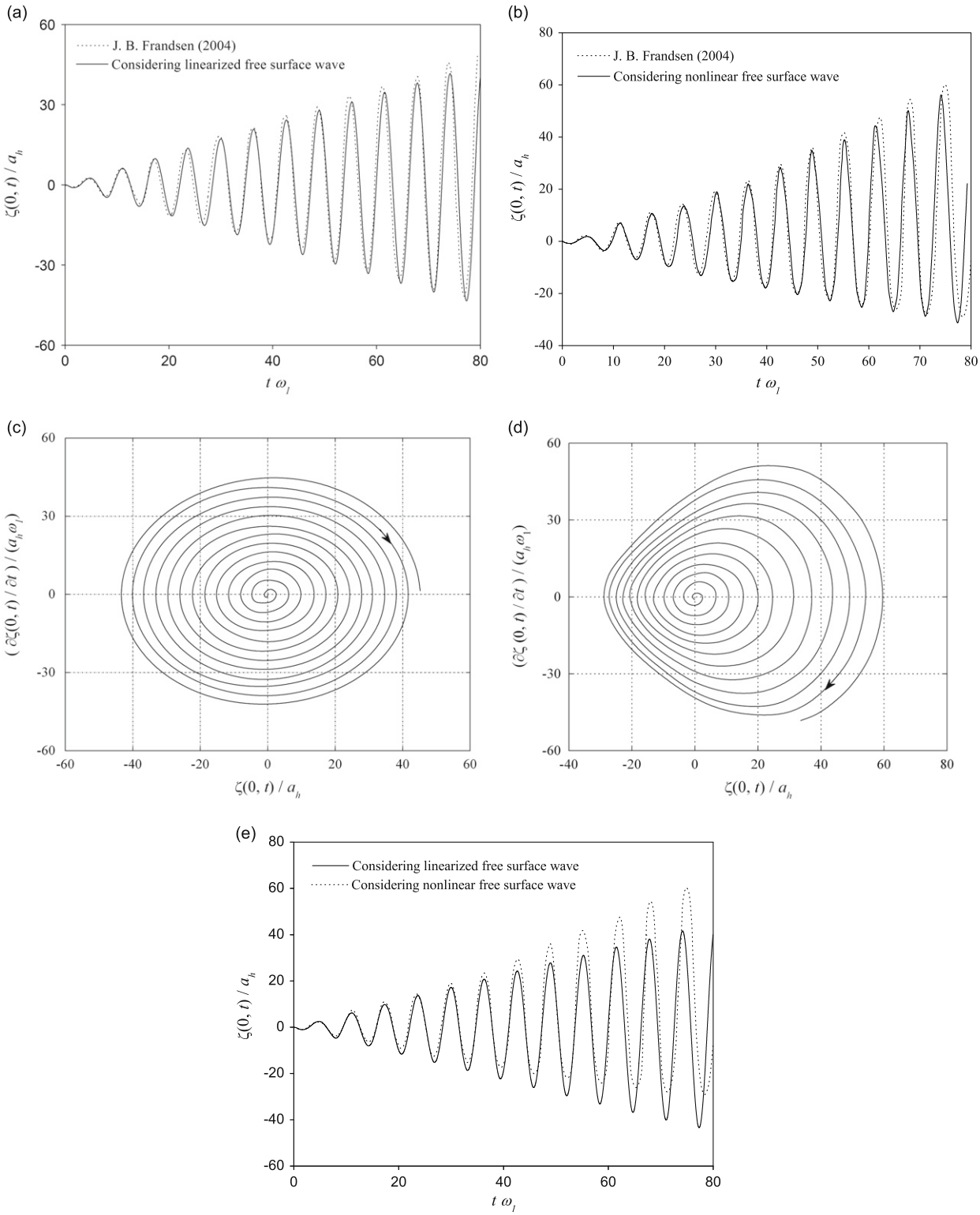

Fig. 9. Free surface elevation at the left wall of container for $\omega_h/\omega_1=1.0$ for smaller horizontal forcing parameter (a) $k_h=0.0014$ and for higher horizontal forcing parameter (b) $k_h=0.014$. The corresponding phase-plots for (c) linear, (d) nonlinear and (e) both linear and nonlinear solutions for large forcing amplitude.

computation. It is also observed that the slosh amplitude increases with time. This phenomenon is occurred if the applied frequency (5.55 rad/s) is close to the natural sloshing frequency (5.548 rad/s).

Example 6. The effect of the nonlinearity of the free surface on the solution of sloshing amplitude is studied by varying the external excitations through the parameter $k_h = a_h\omega_h^2/g$, where a_h and ω_h are the amplitudes and frequencies of external excitations, respectively. The free surface motion is numerically examined at resonance. The results presented are for a container with L=2.0 m and h_l=1.0 m, and considering the external frequency of ω_1=3.76 rad/s, which is close to one of the fundamental sloshing frequency. A time step of 0.003 s is used in the computation. The free-surface elevation at the left wall shown in Fig. 9(a) is for small forcing amplitude (k_h=0.0014) and Fig. 9(b) is for large forcing amplitude (k_h=0.014). It is observed that when the applied amplitude is larger, the nonlinearity of the free surface plays an important role leading to higher peaks, as shown in Fig. 9e. It is clearly shown on the wave phase-plots that the spiral trajectory of the linear solution (Fig. 9(c)) is uniform, whereas the same deforms from cycle to cycle in the nonlinear case (Fig. 9(d)). The same phenomena may be observed in Fig. 9(e). The responses shown in Fig. 9 are compared with the reported results by Frandsen [15]. The same problem was solved earlier by Wu et al. [10] using finite element method. In Fig. 9(a), the magnitude of ζ/a_h reaches about 30 at $t\omega_1$=50 whereas it reaches 35 in Fig. 9(b). If the computational time is increased the magnitude of ζ/a_h reaches about 45 at $t\omega_1$=80 in Fig. 9(a) whereas the magnitude reaches 60 in Fig. 9(b). The trend of sloshing waves is not observed beyond the computational time. However, it does not imply that the variable-amplitude will tend to infinity with time. The result presented here is due to $\Delta\omega=|\omega_1-\omega_0|$=0.001 being very small, which leads to a very long period ($2\pi/\Delta\omega \approx 6280$) and very large amplitude of the wave envelope, where ω_0 is the first fundamental sloshing frequency of the container liquid.

4. Experimental study

The liquid sloshing in partially filled liquid containers is of concern to the researchers of aerospace, civil, nuclear field and several others. Understanding of any complex physical phenomenon like sloshing is enhanced by the use of experimental study to a great extent. Experimental studies help to check the validity of assumptions of the mathematical model and to employ the model effectively for treating container configurations on the basis of their design considerations. In the present work, an experimental arrangement is set up to have an insight of some basic aspects of sloshing phenomenon and to verify the parametric relationships with those of numerical computations. This section presents a detail description of the experimental set-up and the measurement techniques used in the present investigation.

The experimental studies were carried out by different researchers (Abramson [9], Hunt and Priestley [22], Okamoto and Kawahara [23], Pal et al. [11] and Akyildiz and Unal [24,25]) to determine the liquid natural frequencies and the resulting slosh forces in liquid filled rigid containers. The experimental set-up was used in the investigation for measuring slosh induced parameters comprises of a shaking platform for supporting and exciting the test containers along with the associated instrumentation for capturing the desired response. Review of literature reveals a variety of experimental techniques for supporting and oscillating tank models (laboratory scale models) to induce liquid sloshing motions. In the present investigation an already fabricated shaker table having only unidirectional motion is used for the study. The driving mechanism of a lathe machine is a typical mechanical system which permits variations in the amplitude and frequency of oscillations. The table acting as a platform is supported on rollers with guided movement using spring attachments. A cam mechanism is used to transform the circular motion of the machine into a linear movement of the platform. The amplitude of the external excitation may be selected by adjusting the eccentricity of the connecting rod. Maximum possible amplitude in this shaking table is 0.06 m. A prismatic tank model of size 0.50 m in width, 0.35 m in breadth and 0.40 m in height, made of perspex, is fixed to the platform through a fixing arrangement. These dimensions are considered similar to ones, available in literature [9] for comparison. It may be noted that the transparent prismatic tank partially filled with water used in the present experiment is primarily aimed at visual observation of the sloshing modes. The photograph of the experimental arrangement and the instrumentation are shown in Fig. 10.

The wave height measuring probes along with the amplifier developed in house are used to measure the sloshing displacement at various locations on the liquid free surface. These probes are used in conjunction with a signal processing unit where the capacitance values are transduced to a voltage signal between 0 and 10 V. The capacitance variation is a function of the submerged area of the probe and hence varies linearly with the wave height. Voltage signal from the probes are amplified using the amplifier system and the amplified signals are scanned and recorded in a 16-channel HP Bench link data-logger system. All data are stored in a personal computer of P4 series with 512 MB RAM.

4.1. Measurement of slosh displacements

Sloshing height is measured using the capacitance probe at different locations into the container subjected to different excitations. Fig. 11 shows the position of two probes in different positions in the prismatic tank during experiment and the photograph of the typical arrangement of these probes is shown in Fig. 12. The slosh amplitudes are measured and presented in the form of amplitude to tank width ratio (ζ/L). The sloshing amplitudes are measured at the probe positions 1 and 2, however, the results are presented at any one of the probe position. Fig. 13 shows the sloshing height at the probe position 1 in container for depth ratio h_l/H equal to 0.25, subjected to sinusoidal horizontal base excitation with 0.0025 m

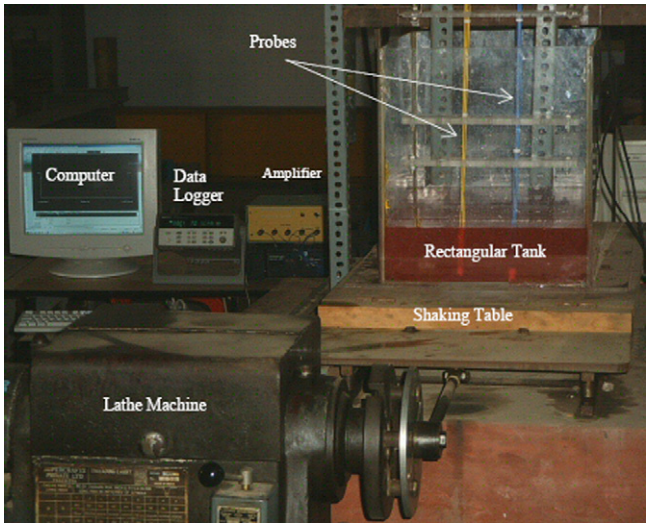

Fig. 10. Experimental arrangement and the instrumentation.

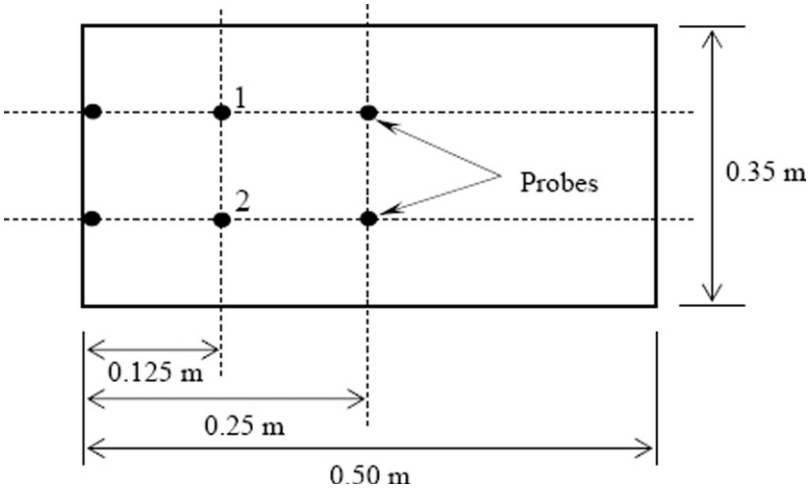

Fig. 11. Position of probes—a plan view.

amplitude and a frequency of 5.236 rad/s. Fig. 14 shows the sloshing height at the probe position 1 for the same amplitude and h_l/H ratio, but with the another excitation frequency of 7.854 rad/s.

The electrical signals are continuously recorded with the help of a 16-channel data acquisition system. Numerical experiments are also carried out in two-dimension considering the same input data. Comparison between the present experimental and numerical results of the free surface slosh amplitude near the container wall is shown in Figs. 13 and 14. It is observed that after each cycle of oscillation, the movement stalls for a small time and again liquid starts oscillating. This is caused due to dissipation of energy. It is observed that the computed sloshing amplitudes are out of phase from the experimental data at certain time. However, the pattern of movement stalls is trivially matched. The deviation in the computed sloshing displacement is due to ineptness of the experimental set-up and the input parameters. As the tank oscillates, different sloshing waves are created depending on the liquid depth and external excitation.

4.2. Measurement of slosh frequencies

Liquid sloshing is a result of the motion of partially filled tank. As the tank moves, it supplies energy to sustain the liquid motion. If the frequency of the tank motion is close to one of the natural frequencies of the liquid, large sloshing amplitude

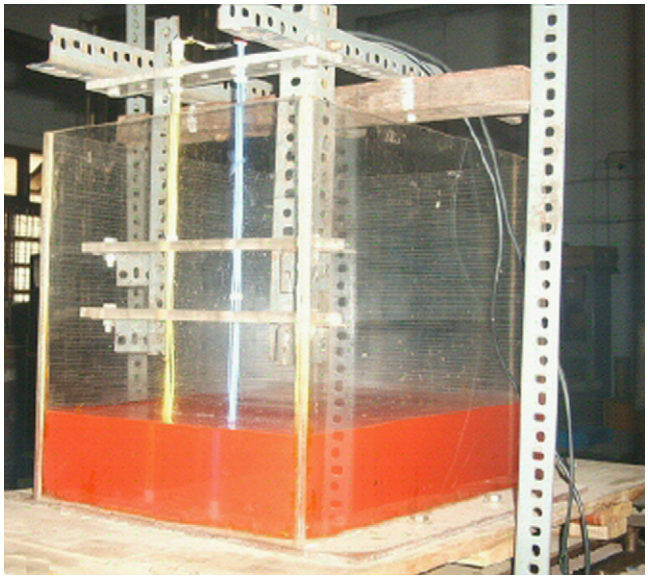

Fig. 12. Typical arrangement of sensors.

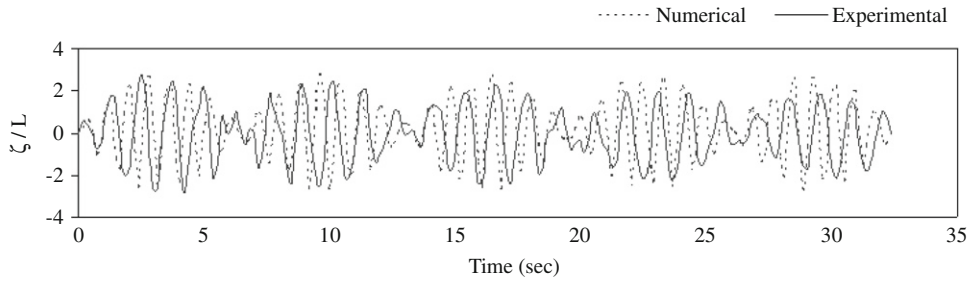

Fig. 13. Comparison of experimental and numerical (MLPG) results for the frequency of 5.236 rad/s.

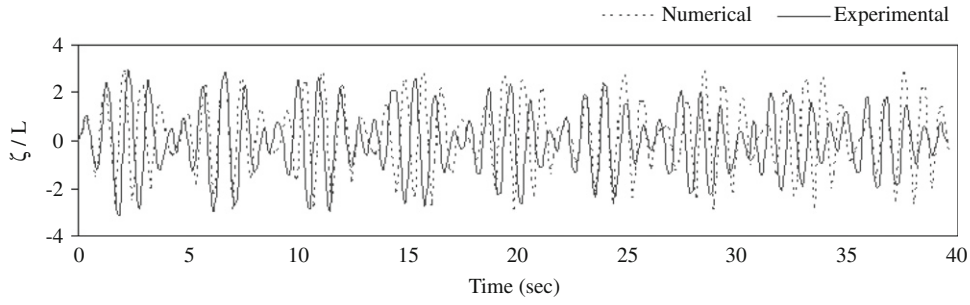

Fig. 14. Comparison of experimental and numerical (MLPG) results for the frequency of 7.854 rad/s.

occurs. For a given prismatic tank, the natural frequencies of the liquid depending on the fill depth are obtained from the expression [9] as given below:

$$\omega_{ns}^2 = \left(\frac{g\xi}{4\pi}\right)\tanh(\pi h_l \xi) \quad \text{and} \quad \xi = \sqrt{\left(\frac{m}{a}\right)^2 + \left(\frac{n}{b}\right)^2} \tag{25}$$

where m or n is the number of half-waves in the X- or - Z direction, h_l is the liquid depth, a and b are the lengths of the sides of the container. The general technique to measure the liquid natural frequency is to oscillate the tank at low amplitude

and then stop the oscillation and record the frequency at which the undistorted wave shape reaches the maximum amplitude without rotation. The experimentally measured values of the first natural sloshing frequency for the test model tank for different depths of liquid are presented in Table 2. The results are compared with the reported results published by Abramson [9]. It is observed that the experimental results are closer to the one indicated in the literature. However, a little variation is observed while comparing with the present numerical results and the percentage error varies within 4% between the experimental and the present numerical results. These results may be regarded as satisfactory considering various limitations and approximations made during the experimental measurements.

Table 2
Comparison of natural slosh frequency (rad/s) for different depth ratios.

Depth ratio (h_l/H)	Present MLPG values in 2-D tank ω	Abramson [9] ω_n	Present experimental values ω_{ns}
0.175	5.0212	4.959	4.9587
0.200	5.1231	–	5.1491
0.225	5.3243	5.236	5.2346
0.250	5.4977	–	5.3267

Table 3
The non-dimensional slosh amplitude with the change in depth ratio for different external amplitude.

h_l/H	ζ/L	
	a_h=0.0025 m	a_h=0.005 m
0.125	0.01	0.019
0.15	0.03	0.183
0.175	0.164	0.287
0.2	0.103	0.135
0.225	0.103	0.155
0.25	0.072	0.125
0.275	0.06	0.174
0.3	0.019	0.064
0.325	0.021	0.064

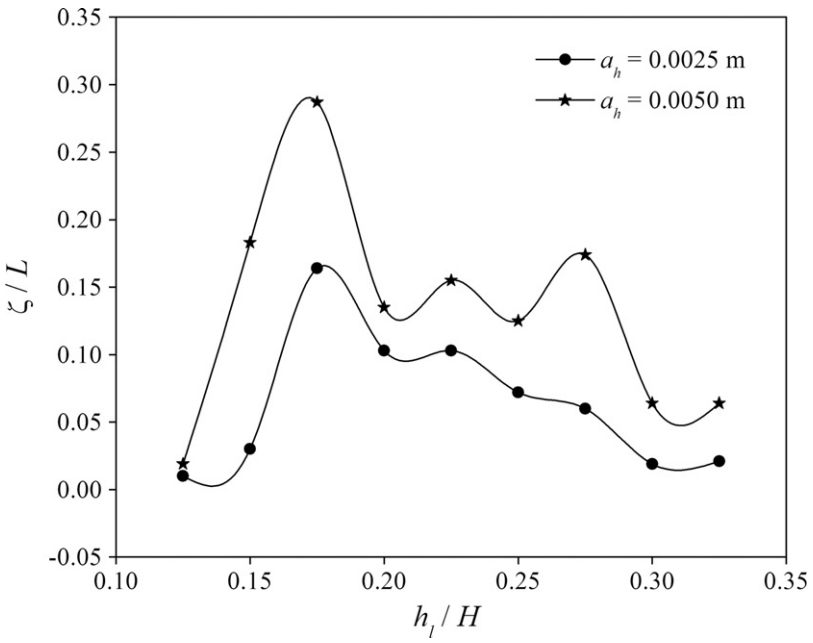

Fig. 15. Non-dimensional slosh height with various liquid depths for different applied amplitudes without changing the applied frequency.

4.3. Parametric study

The selected tank is considered for the present experimental investigation. The capacitance probe is used to measure the variation of slosh amplitude at different locations inside the tank. The different probe positions into the container are $-0.5L$, $-0.25L$, 0, $+0.25L$ and $+0.5L$, respectively (Fig. 11). Centerline of the tank is taken as reference line. Tank is examined for different depths of liquid. A few cases are presented here to observe the variation of non-dimensional slosh amplitude with the change in depth ratio, amplitude and frequency of applied acceleration. Where depth ratio (h_l/H)= depth of liquid into the tank/height of the tank, and non-dimensional slosh amplitude (ζ/L)=sloshing height at a particular point/width of the tank.

4.4. Variation of slosh amplitude due to change in depth ratio

The slosh amplitude is measured for different depths of liquid (water) into the selected tank. The non-dimensional slosh amplitude with the change in depth ratio for different external amplitude is presented in Table 3 and the results are plotted in Fig. 15 for different external amplitude without changing the frequency of 5.236 rad/s. It is observed that the applied amplitude increases with the increase in slosh amplitude. The non-dimensional slosh amplitude with the change in depth ratio for different external frequency is presented in Table 4 and the results are plotted in Fig. 16 without changing the external amplitude of 0.005 m. It is observed that the excitation frequency increases with the decrease in slosh amplitude.

Table 4
The non-dimensional slosh amplitude with the change in depth ratio for two different applied frequencies.

h_l/H	ζ/L	
	ω_h=5.236 s^{-1}	ω_h=7.854 s^{-1}
0.1	0.063	0.023
0.125	0.072	0.183
0.15	0.083	0.285
0.175	0.044	0.135
0.2	0.042	0.155
0.225	0.014	0.127
0.25	0.043	0.175
0.275	0.015	0.064

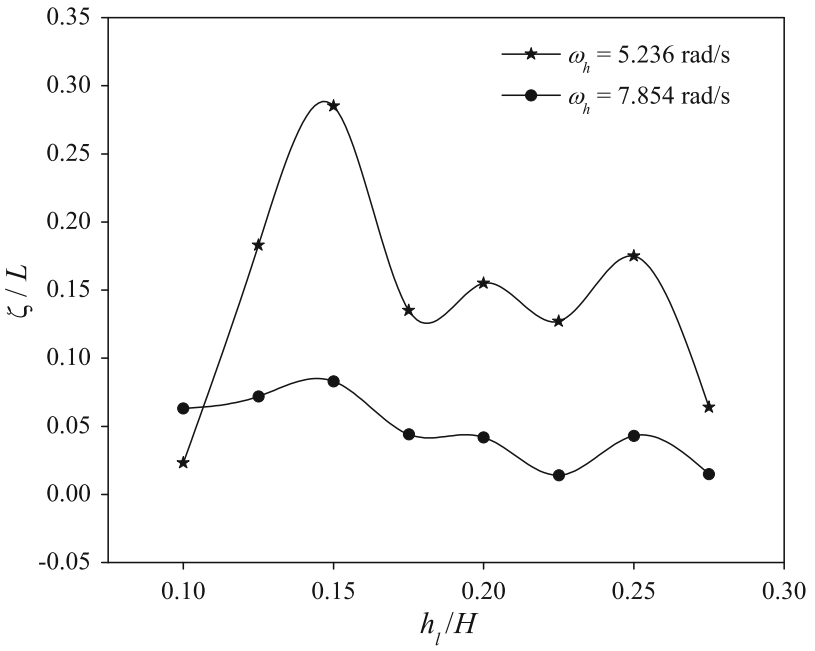

Fig. 16. Non-dimensional slosh height with various liquid depths for different applied frequencies without changing the applied amplitude.

Table 5
The non-dimensional slosh amplitude with the change in depth ratio for different external frequency.

ω_h (s^{-1})	ζ/L			
	h_l/H=0.175	h_l/H=0.225	h_l/H=0.275	h_l/H=0.325
5.236	0.04	0.14	0.05	0.05
7.854	0.01	0.03	0.08	0.11
11.6	0.04	0.02	0.02	0.00
17.9	0.14	0.18	0.26	0.16

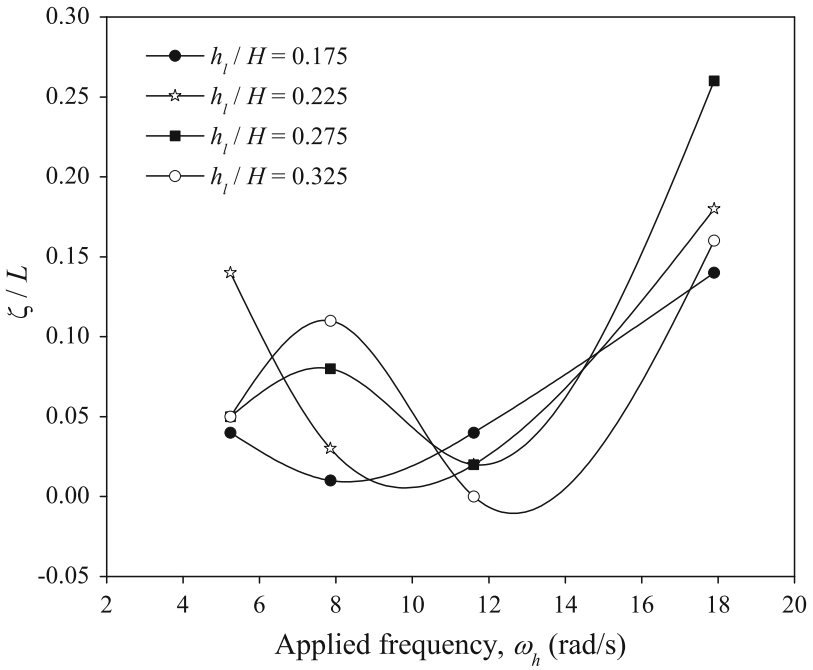

Fig. 17. Variation of non-dimensional slosh height with applied frequency for different liquid depths.

Further, increase in liquid depth causes decrease in slosh amplitude. However, for a particular value of depth ratio (0.15), it is showing a local peak value. This may be due to the closeness of external frequency to one of the fundamental slosh frequencies of the container liquid. The non-dimensional slosh amplitude with the change in depth ratio for different external frequency is presented in Table 5 and the results are plotted in Fig. 17 for a particular applied amplitude of 0.005 m. It is observed that slosh amplitude follows sinusoidal pattern because of sinusoidal nature of applied external excitation.

4.5. Variation of slosh amplitude due to change in excitation

Several numerical models at various sloshing amplitudes due to change in applied excitations were proposed by Wu et al. [10]. However, in the present experimental investigation, the slosh amplitudes are measured for different external excitations. The selected tank model is examined for a particular depth of liquid to observe the change in sloshing amplitude with varying applied frequencies and amplitudes. The depth of liquid is 0.13 m. The non-dimensional slosh amplitude at different applied amplitude with the change in applied frequency is presented in Table 6 and the results are plotted in Fig. 18. It is observed that the slosh amplitude follows sinusoidal pattern, i.e. slosh amplitude increases initially with the increase of applied frequency and thereafter it decreases and again with the increase in external frequency slosh amplitude increases. This is because of sinusoidal nature of applied external excitation on the liquid-filled container. The non-dimensional slosh amplitude with the change in depth ratio for different external amplitude is presented in Table 7 and the results are plotted in Fig. 19 for a constant applied frequency of 5.236 rad/s. It is observed that the slosh amplitude increases with the increase in applied amplitude. However, slosh amplitude decreases with the increase in liquid depth. The selected tank is examined after sudden release of external excitation, which is shown in Fig. 20. The depth of liquid is

Table 6
The non-dimensional slosh amplitude for different applied amplitude with the change in applied frequency.

ω_h (s^{-1})	ζ/L				
	a_h=0.0025 m	a_h=0.005 m	a_h=0.0075 m	a_h=0.01 m	a_h=0.0125 m
5.236	0.02	0.05	0.05	0.06	0.11
7.854	0.06	0.11	0.12	0.16	0.28
11.6	0.00	0.00	0.00	0.02	0.08
17.9	0.16	0.16	0.16	0.16	0.36

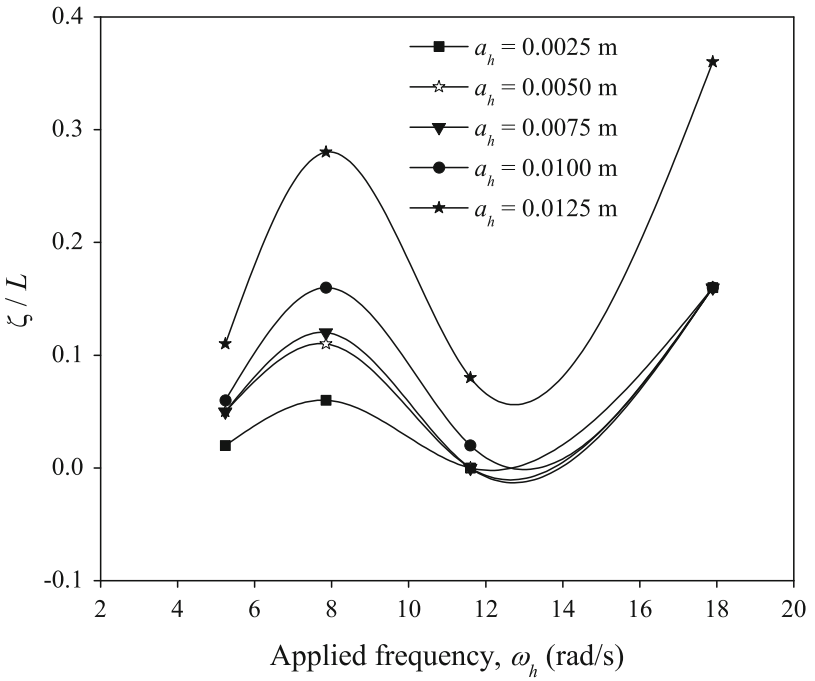

Fig. 18. Variation of non-dimensional slosh height with applied frequency for different applied amplitudes.

Table 7
The non-dimensional slosh amplitude with the change in depth ratio for different external amplitude.

a_h (m)	ζ/L			
	h_l/H=0.225	h_l/H=0.275	h_l/H=0.325	h_l/H=0.4
0.0025	0.06	0.02	0.02	0.01
0.005	0.14	0.02	0.05	0.02
0.0075	0.22	0.10	0.05	0.05
0.01	0.22	0.32	0.06	0.06

0.09 m, applied frequency is 5.236 rad/s and applied amplitude is 0.005 m. It is observed that the slosh amplitude decreases exponentially with time.

5. Conclusions

A meshless formulation is developed to compute the nonlinear sloshing amplitude of liquid in liquid-filled prismatic containers subjected to sinusoidal base excitation. The Petrov–Galerkin method has been used to obtain the solution. Both the numerical and experimental studies of sloshing of liquid in partially filled containers are presented here. The validity and accuracy of the present numerical solution procedures is checked by comparing the nonlinear sloshing response of

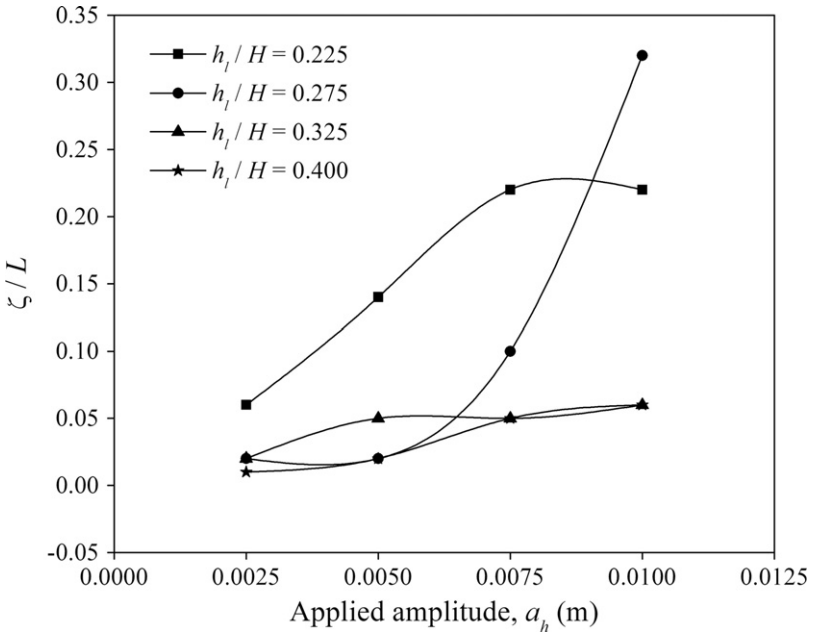

Fig. 19. Variation of non-dimensional slosh height with applied amplitude for different liquid depths.

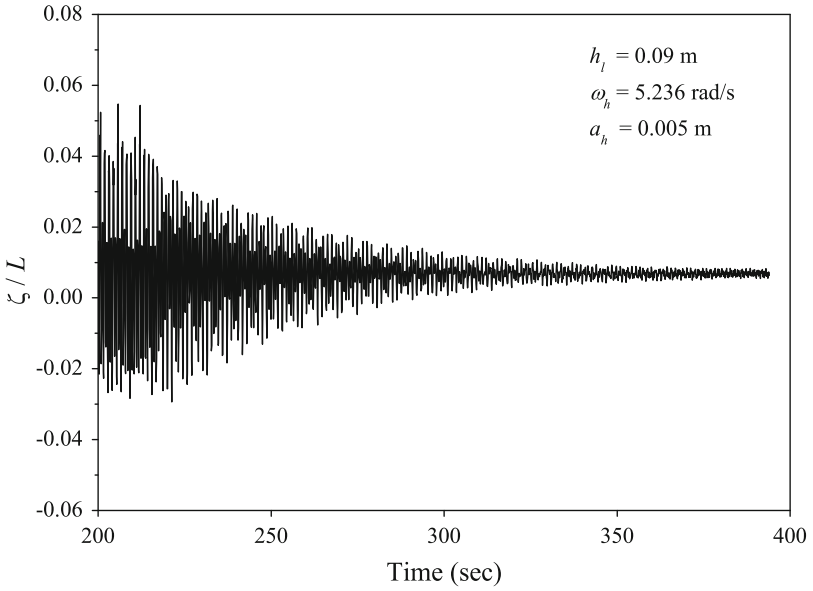

Fig. 20. Non-dimensional sloshing amplitude after offing the external excitation.

liquid in liquid-filled containers with the existing solutions [15,21] and a good agreement is found. It can be noted that the slosh characteristics are strongly influenced by the tank geometry, depth of liquid, and the amplitude and frequency of external excitation. The effect of free surface nonlinearity on the sloshing response appears to be significant when the amplitude of excitation becomes large and the frequency of excitation approaches to the immediate neighborhood of a natural free-surface frequency of the liquid. In the experimental study, for a particular depth of liquid in container subjected to sinusoidal base excitation, it is observed that after each cycle of oscillation, the liquid movement stalls for a small time and again liquid starts oscillating due to dissipation of energy. The numerical results are not matching exactly with those obtained experimentally and the variations in the data may be due to inadequancies of the experimental set-up and the input parameters. Tracing of free surface sloshing, the MLPG method based on LSWF is found to be simple and attractive with a great potential in engineering applications.

References

[1] J.J. Monaghan, An introduction to SPH, *Computer Physics Communications* 48 (1) (1988) 89–96.
[2] B. Nayroles, G. Touzot, P. Villon, Generalizing the finite element method: diffuse approximation and diffuse elements, *Computational Mechanics* 10 (1992) (1992) 307–318.
[3] T. Belytschko, Y.Y. Lu, L. Gu, Element-free Galerkin methods, *International Journal for Numerical Methods in Engineering* 37 (1994) 229–256.
[4] W.K. Liu, Y. Chen, C.T. Chang, T. Belytschko, Advances in multiple scale kernel particle methods, *Computational Mechanics* 18 (73) (1996) 73–111.
[5] I. Babuska, M. Melenk, The partition of unity method, *International Journal for Numerical Methods in Engineering* 40 (1997) 727–758.
[6] S.N. Atluri, T. Zhu, A new meshless local Petrov–Galerkin (MLPG) approach in computational mechanics, *Computational Mechanics* 22 (1998) 117–127.
[7] S.N. Atluri, S. Shen, in: *The Meshless Local Petrov–Galerkin (MLPG) Method*, Tech. Science Press, 2002 382 pp.
[8] S.N. Atluri, S. Shen, The meshless local Petrov–Galerkin (MLPG) method: a simple and less-costly alternative to the finite element and boundary element methods, *Computer Modeling in Engineering and Sciences* 3 (1) (2002) 11–51.
[9] H.N. Abramson, The dynamic behavior of liquids in moving containers, *NASA SP-106*, National Aeronautics and Space Administration, Washington, DC, 1966.
[10] G.X. Wu, Q.W. Ma, Taylor R. Eatock, Numerical simulation of sloshing waves in a 3D tank based on finite element method, *Applied Ocean Research* 20 (1998) 337–355.
[11] N.C. Pal, S.K. Bhattacharyya, P.K. Sinha, Experimental investigation of slosh dynamics of liquid-filled containers, *Experimental Mechanics* 41 (1) (2001) 63–69.
[12] N.C. Pal, S.K. Bhattacharyya, P.K. Sinha, Nonlinear coupled slosh dynamics of liquid-filled laminated composite containers: a two dimensional finite element approach, *Journal of Sound and Vibration* 261 (2003) 729–749.
[13] M.S. Celebi, H. Akyildiz, Nonlinear modeling of liquid sloshing in a moving rectangular tank, *Ocean Engineering* 29 (2002) 1527–1553.
[14] K.C. Biswal, S.K. Bhattacharyya, P.K. Sinha, Free-vibration analysis of liquid-filled tank with baffles, *Journal of Sound and Vibration* 259 (1) (2003) 177–192.
[15] J.B. Frandsen, Sloshing motions in excited tanks, *Journal of Computational Physics* 196 (1) (2004) 53–87.
[16] Q.W. Ma, Meshless local Petrov–Galerkin method for two-dimensional nonlinear water wave problems, *Journal of Computational Physics* 205 (2005) 611–625.
[17] Q.W. Ma, MLPG method based on Rankine source solution for simulating nonlinear water waves, *Computer Modeling in Engineering and Sciences* 9 (2) (2005) 193–210.
[18] K.C. Biswal, S.K. Bhattacharyya, P.K. Sinha, Non-linear sloshing in partially liquid filled containers with baffles, *International Journal for Numerical Methods in Engineering* 68 (2006) 317–337.
[19] Q.W. Ma, A new meshless interpolation scheme for MLPG_R method, *Computer Modeling in Engineering and Sciences* 23 (2) (2008) 75–90.
[20] Q.W. Ma, J.T. Zhou, MLPG_R method for numerical simulation of 2D breaking waves, *Computer Modeling in Engineering and Sciences* 43 (3) (2009) 277–304.
[21] K. Washizu, T. Nakayama, M. Ikegawa, Y. Tanaka, T. Adachi, Some finite element techniques for the analysis of non-linear sloshing problems, *Finite Elements in Fluids* 5 (1984) 357–376.
[22] B. Hunt, N. Priestley, Seismic water waves in a storage tank, *Bulletin of the Seismological Society of America* 68 (2) (1978) 478–499.
[23] T. Okamoto, M. Kawahara, Two-dimensional sloshing analysis by Lagrangian finite element method, *International Journal for Numerical Methods in Engineering* 11 (1990) 453–477.
[24] H. Akyildiz, N.E. Unal, Experimental investigation of pressure distribution on a rectangular tank due to the liquid sloshing, *Ocean Engineering* 32 (2005) 1503–1516.
[25] H. Akyildiz, N.E. Unal, Sloshing in a three-dimensional rectangular tank: numerical simulation and experimental validation, *Ocean Engineering* 33 (2006) 2135–2149.